Abiotic Degradation and Composting Behavior of 3D-Printed PLA and PLA/Wood Biocomposites

A.A. Pérez-Fonseca[1], M.R. Gómez-Comparán[2], Y. González-García[2], A. Barajas-Cervantes[1], J.A. Silva-Guzmán[2] and J.R. Robledo-Ortíz[2,*]

[1]*Departamento de Ingeniería Química, Universidad de Guadalajara, Jalisco, México*

[2]*Departamento de Madera, Celulosa y Papel, Universidad de Guadalajara, Jalisco, México*

Abstract: The use of 3D printing technology is growing due to its ease of use, accessibility, and potential to produce complex and functional products. In the construction and building industries, 3D printing is used to produce intricate enclosures, building components, furniture designs, and household items. However, the accessibility of this technology is accompanied by the generation of polymeric residues, especially poly(lactic acid) (PLA), which is also prone to abiotic degradation. In this context, the present work aims to analyze the abiotic degradation and composting behavior of 3D-printed PLA and its wood biocomposite. The printed materials were subjected to accelerated weathering and characterized in terms of their physical and mechanical properties, as well as their surface chemical changes via FTIR. Additionally, disintegration and mineralization under composting conditions were evaluated, including a preliminary assessment of microplastics generation. The results showed that, as expected, the initial porosity was higher in the biocomposite (12.5%) than in the neat PLA (7.5%); however, after weathering, it increased to 13.2% in the pure biopolymer, while the biocomposite remained almost unaffected. This behavior is attributed to the wood particles, which inhibited the hydrolysis of PLA under weathering and water immersion. The wood particles also reduced microplastics generation without affecting the ultimate biodegradation, with calculated maximum mineralization values of approximately 75%.

Keywords: Poly(lactic acid), Biocomposites, 3D-printing, Degradation, Composting.

1. INTRODUCTION

3D printing is now a widely accessible and popular manufacturing technology. Among the various techniques available, fused deposition modeling (FDM) is one of the most commonly used. This process involves the use of filaments, such as poly(lactic acid) (PLA), to produce custom-designed objects, often not commercially available, using models created in computer-aided design (CAD) software, without the need for molds (Bhagia *et al*., 2021).

The 3D printing of thermoplastics has rapidly gained attention in the construction and building industries, particularly with the adoption of “Digital Materiality” and the capability to fabricate complex enclosures and other building components (Gramazio *et al*., 2014; Yin *et al*., 2018). Ning *et al*. (2021) conducted a literature review reporting that publications on 3D printing in construction increased from just 3 in 2012 to 109 in 2020, reflecting the growing relevance of this technology in the field. Furthermore, 3D printing has also expanded into the design of complex furniture and its components, as well as household items and their repair (Jain and Jain, 2021; Yang and Du, 2022).

A variety of polymers and biopolymers can now be processed using 3D printing, with the most common being poly(lactic acid) (PLA), acrylonitrile butadiene styrene (ABS), polycarbonate (PC), and polyamide (PA). Among them, PLA is the most used thermoplastic in 3D printing due to its favorable properties, including low cost, availability in various grades and melt flow indices, biodegradability, and renewable bio-based origin (Joseph *et al*., 2023). Also, PLA/natural fibers biocomposites are being used and studied. Bhagia *et al*. (2021) conducted a review on 3D printing of PLA-based biocomposites reinforced with biomass resources. They reported that, as expected, cellulose, hemicellulose, lignin, and whole biomass modify the mechanical strength, reduce production costs, and improve renewability and the carbon footprint, as biomass can be derived from agro-industrial waste. Petchwattana *et al*. (2019) developed PLA filaments incorporating rubber and teak wood flour, using silane as a coupling agent for 3D printing applications. The silane treatment was found to improve the interfacial compatibility between the matrix and the fibers, resulting in enhanced mechanical properties. Figueroa-Velarde *et al*. (2021) produced PLA filaments with agave fibers to fabricate 3D-printed biocomposites. They reported that increasing fiber content led to higher porosity, which in turn reduced flexural and tensile properties. Additionally, they found that the printing angle significantly affected both morphology and mechanical performance, with a 45° printing angle yielding the best mechanical properties.

However, the widespread use of 3D printing inevitably leads to an increasing amount of waste

*Address correspondence to this author at the Departamento de Madera, Celulosa y Papel, Universidad de Guadalajara, Jalisco, México;
E-mail: jorge.robledo@academicos.udg.mx

Received on 05-07-2025 Accepted on 15-08-2025 Published on 19-08-2025

E-ISSN: 2819-828X/25

associated with the process, especially in cases such as rapid applications, household items, and even novice users with trial-and-error productions. González-López *et al*. (2020) observed that PLA and its biocomposites subjected to accelerated weathering primarily lose their mechanical performance due to degradation of their amorphous regions, which are more susceptible to hydrolysis. Additionally, the lignin present in the fibers absorbs between 80% and 95% of UV radiation, which also contributes to material degradation through oxidation and structural breakdown. Lin *et al*. (2019) processed wood flour/PLA biocomposites using 3D printing and exposed them to accelerated weathering. They observed that higher temperatures accelerated the aging process and that the tensile strength decreased by up to 44% in the weathered biocomposites compared to unexposed materials.

On the other hand, the biodegradation of PLA and its biocomposites requires specific abiotic conditions and interaction with microorganisms, which occur in composting processes. Conditions such as humidity, temperature, and enzymatic activity promote the scission of polymer chains, resulting in weight loss and the release of oligomers, dimers, and monomers. These degradation products are subsequently utilized by microorganisms as sources of carbon and energy, leading to the formation of biomass and the production of metabolites such as CO_2, methane, and water, depending on whether the process is aerobic or anaerobic. This biochemical transformation is known as mineralization (Lucas *et al*., 2008). In the case of biocomposites, Meereboer *et al*. (2020) found that their biodegradation can be enhanced or restricted depending on the composition of the natural fibers. Moreover, inorganic additives such as antifouling agents and plasticizers may inhibit the biodegradation process. If biodegradation does not occur under appropriate conditions, it can lead to the formation of undesirable byproducts, including potentially toxic compounds, polymer waste accumulation, or the generation of microplastics (Andrady, 2017; Benhami *et al*., 2024).

In this context, it is essential to study the abiotic and biotic degradation processes of these materials to better understand their medium- and long-term performance and potential environmental impacts. This study aimed to evaluate the degradation behavior of PLA and PLA/wood biocomposites processed by 3D printing under accelerated weathering and composting conditions. To this end, the materials were characterized based on their physical and mechanical properties, surface functional group changes, and biodegradation performance through respirometry tests.

2. MATERIALS AND METHODS

2.1. Materials

The filaments used were PLA+ and PLA+ 20% w/w wood flour (sandalwood), both from the brand iSANMATE® (China), 1.75 mm diameter, 190-225 °C print temperature, and 30-600 mm s^{-1} print speed. The use of PLA+ and PLA+ blends is preferred over conventional PLA for 3D-printed structures intended for better performance, since PLA+ filaments include additives that improve their processability, properties, and, importantly, durability.

2.2. Processing by 3D Printing

The PLA+ and PLA+/wood flour (BC) filaments were processed using a Guider II Flashforge 3D printer. The printing conditions were 210 °C extruder temperature, 30 °C bed temperature, 60 mm s^{-1} printing speed, 100% infill density with a line pattern (initial angle 0° and crossing angle 90°). The specimens for the various characterization tests were obtained directly through this processing technique, following the corresponding standard. All digital models were designed using a Fusion 360 software.

2.3. Accelerated Weathering

The 3D printed samples were subjected to accelerated weathering using a QUV Basic machine to evaluate the abiotic degradation effect on their properties. These samples were exposed to cyclic conditions consisting of 2 h of UV light exposure, 2 h of water condensation, and a constant temperature of 55 °C for a total duration of 600 h, following ASTM G154.

2.2. Morphology, Porosity, Color, and Dimensional Stability

The morphology of the materials was analyzed using a Hitachi TM-1000 scanning electron microscope (SEM). A qualitative characterization of the material morphology was performed before and after weathering, as well as during the composting process, using optical images obtained with a Nikon DSLR D5500 camera and an AF-S Micro Nikkor 85 mm macro lens.

Real density (ρ_r) measurements were carried out using a Quantachrome Instruments Ultrapyc 1200e gas pycnometer with nitrogen, while bulk density (ρ_b) was determined according to ASTM D2395. The porosity of the materials was calculated using Equation 1:

$$Porosity\ (\%) = \left(1 - \frac{\rho_b}{\rho_r}\right) \times 100 \quad (1)$$

Color changes were determined using the CIE*Lab* system with a portable WR-10 colorimeter. This system is based on RGB chromatic coordinates, and the total color difference (Δ*E*) was calculated using Equation 1:

$$\Delta E = \sqrt{\Delta L^2 + \Delta a^2 + \Delta b^2} \quad (2)$$

where Δ*L* represents a change in the lightness (less luminosity), Δ*a* indicates a shift between red and green tones, and Δ*b* indicates a shift between yellow and blue tones.

2.3. FTIR-ATR Spectroscopy

Chemical changes on the surface of the materials were determined by FTIR-ATR using a Thermo Scientific Nicolet iS5 spectrometer, with a resolution range of 4000 to 400 cm^{-1}. Additionally, the level of degradation was quantified by determining the carbonyl index (CI), calculated using Equation 3:

$$CI = \frac{I_{C=O}}{I_{C-H}} \quad (3)$$

where $I_{(C=O)}$ is the area under the curve of the carbonyl group (1750 cm^{-1}), and $I_{(C-H)}$ is the area under the C–H stretching band (2800–3000 cm^{-1}) (Martín del Campo *et al.*, 2021). This test was performed before and after exposing the specimens to accelerated weathering.

2.4. Differential Scanning Calorimetry (DSC)

Thermal properties of the materials before and after exposure to accelerated weathering were obtained using a TA Instruments Discovery Q100 system. The equipment was programmed for a temperature range of 25 to 200 °C at a heating rate of 10 °C min^{-1}, with a nitrogen flow rate of 50 mL min^{-1}. Samples of approximately 4 mg were prepared in aluminum pans. The degree of crystallinity (X_c) was determined using Equation 4:

$$X_c\ (\%) = \left(\frac{\Delta H_m - \Delta H_c}{\Delta H_{ref}}\right) \times \frac{1}{x} \times 100 \quad (4)$$

where ΔH_m is the heat of fusion, ΔH_c is the cold crystallization, and ΔH_{ref} is the theoretical heat of fusion of fully crystalline neat PLA (93 J g^{-1}). The variable *x* represents the PLA fraction in the material (weight fraction).

2.5. Mechanical Characterization

The mechanical characterization of the materials was carried out before and after accelerated weathering to assess abiotic degradation indirectly. Flexural properties were determined according to ASTM D790 using an Instron 4411 universal testing machine with specimens measuring 70 × 12.7 × 3 mm^3 and a crosshead speed of 2 mm min^{-1}. Tensile tests were conducted following the ASTM D638 using type IV specimens and a strain rate of 5 mm min^{-1} on an Instron 3345 universal testing machine. Finally, impact strength was measured according to ASTM D6110 using specimens of 127 × 12.7 × 3 mm^3 on an Instron Ceast 9050 impact tester. In all cases, average values and standard deviations are reported as specified in the corresponding standard.

2.6. Water Absorption

Water absorption capacity was determined according to ASTM D570. PLA is particularly susceptible to hydrolytic degradation, making it essential to characterize this process. Water absorption was calculated using Equation 5:

$$Water\ absorption\ (\%) = \left(\frac{W_i - W_0}{W_0}\right) \times 100 \quad (5)$$

where W_0 is the dry weight of the sample and W_i is the weight of the sample after being immersed for a time *t*. This test was also conducted before and after exposing the specimens to accelerated weathering. The samples were submerged in distilled water in closed jars and kept at 55 °C. During the initial phase, measurements were taken at 2, 4, 6, 24, and 48 h, removing excess water using a microfiber towel and weighing the samples. Afterwards, samples were weighed every 7 days until the end of the 42-day testing period. At the end of the experiment, the weight difference and mass loss due to the hydrolysis of PLA were determined using Equation 6:

$$WL_{hydrolysis}\ (\%) = \left(\frac{h_f - h_0}{h_0}\right) \times 100 \quad (6)$$

where h_0 is the dry weight of the sample before starting the absorption test, and h_f is the final dry weight of the sample.

2.7. Composting and Respirometry

2.7.1. Weight Loss by Composting

Weight loss tests were performed to evaluate the biodegradation of the samples under simulated laboratory-scale composting conditions, following ISO 20200:2004. The samples, measuring 25 × 25 × 3 mm^3, were initially dried in an oven at 60 °C. They were then placed in compost composed of 55% solids (40% sawdust, 30% rabbit manure, 10% mature compost, 10% starch, 5% sucrose, 4% corn oil, and 1% urea) and 45% water, and maintained at 58 °C. One sample was removed after 10 days, followed by additional samples taken every 7 days until day 59, with the final set removed on day 85. After removal, the samples were cleaned, dried in an oven at 60 °C, and weighed.

All experiments were conducted in triplicate. The degree of disintegration (DD) was calculated using Equation 7:

$$DD\ (\%) = \left(\frac{m_i - m_0}{m_0}\right) \times 100 \quad (7)$$

where m_0 is the dry weight of the sample before composting, and m_i is the dry weight of the sample after composting.

Additionally, a preliminary quantification of microplastics in the residual compost was carried out. For this purpose, the residual compost of each of the three replicates from the weight loss experiments was weighed and manually sieved using a 1 mm (1000 µm mesh). This process was carried out to isolate PLA and PLA/wood fragments falling within the microplastic size range of 1 mm to 1 µm. This size range for microplastics was proposed by Van Cauwenberghe *et al*., (2015) and Andrady (2017), who mentioned that the upper size limit of 1 mm is more intuitive and stricter to the micrometer range, while particles under 1 µm are considered nanoplastics. The recovered microplastic samples were sieved a second time using the same 1 mm mesh to disintegrate possible clumps or aggregates and ensure proper size classification. The microplastic content in the residual material (*Mps*) was calculated using Equation 8:

$$Mps\ (\%) = \left(\frac{m_2}{m_1}\right) \times 100 \quad (8)$$

where m_1 is the total mass of the material before sieving, and m_2 is the mass of microplastics recovered. Additionally, optical images with a minimum of 20 particles were measured using the ImageJ software to determine the particle size distribution.

2.7.2. Respirometry

Respirometry tests were performed to assess CO_2 production and the mineralization of the materials during composting, following the ISO 14855-1 standard. The tests used Oxitop C WTW respirometers with an OC 110 controller and an Achat OC software version 3.2. Two controls containing only compost were set to establish a reference for CO_2 generation in the absence of samples. Test specimens measuring 25 × 25 × 3 mm^3 were used, with three samples per composition placed in each respirometer along with 123 g of compost. Measurements were performed in duplicate over 99 days, with the respirometers kept in an incubator at 58 °C. The vessels were opened every 3 days for aeration. A 1 M NaOH solution was used and periodically replaced to absorb the generated CO_2. More details of the experiment are previously reported in Gallardo-Cervantes *et al*., (2021).

The mineralization (y) of the samples was calculated using Equation 9, and the kinetics were fitted to the semi-empirical Hill model (Equation 10) to obtain kinetic parameters.

$$y\ (\%) = \left(\frac{CO_{2\ sample} - CO_{2\ blank}}{\mathrm{Th}CO_2}\right) \times 100 \quad (9)$$

$$y\ (\%) = y_{max} \times \left(\frac{t^n}{k^n + t^n}\right) \quad (10)$$

where ThCO_2 is the theoretical CO_2 that the samples are expected to produce (calculated from the carbon mass fraction obtained through elemental analysis), y_{max} (%) is the maximum mineralization achievable at infinite time t (days), n is a dimensionless parameter that defines the curvature of the sigmoidal function, and k (days) is the half-life, representing the time required to reach 50% of the maximum mineralization. The semi-empirical Hill model has been reported to accurately describe the biodegradation of polymers (La Fuente Arias *et al*., 2024; Da Silva *et al*., 2024).

3. RESULTS AND DISCUSSION

3.1. Morphology and Color Change

The micrographs obtained using scanning electron microscopy (Figure **1**) show the structure of the printed PLA and the biocomposites (BC) before and after exposure to accelerated weathering. High porosity in the structure is evident due to the nature of the processing, which creates gaps between the printed layers. This is clearly visible through the overlapping layers oriented from 0° to 90° and the cross-sectional or longitudinal cuts of the filament. These interlayer gaps significantly increase after the weathering process for both PLA and BC, along with the formation of fractures and voids within the bulk of the materials, resulting from exposure to UV light, temperature, and humidity. Chopra *et al*. (2023) evaluated the atmospheric degradation of 3D-printed PLA and observed significant surface deterioration after 30 days of exposure, which progressed into the bulk of the material by day 45.

Porosity was quantitatively determined through density measurements, as also shown in Figure **1**. The printed PLA exhibited a porosity of 7.5%, while the biocomposite showed a considerably higher value of 12.5%. After accelerated weathering, neat PLA was affected more significantly than the biocomposite, with its porosity increasing to 13.2%. This is because exposure to UV, temperature, and humidity causes cracks in the material, allowing water to enter the interfacial voids between print filaments, as observed in SEM micrographs. The lower susceptibility of the biocomposite can be attributed to a reduced exposed PLA area due to the presence of wood, which may also

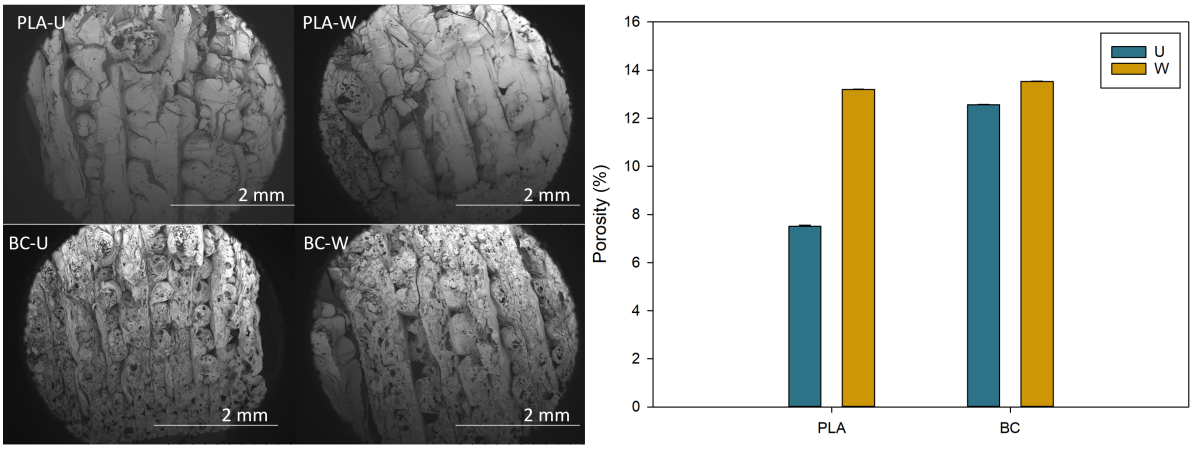

Figure 1: SEM micrographs and porosity of 3D-printed PLA and BC before (U) and after (W) accelerated weathering.

absorb some UV radiation via the chromophore groups in its lignin. Lin *et al*. (2019) also reported increased porosity in non-printed PLA/poplar wood flour filaments exposed to UV light.

Color changes in the materials after accelerated weathering and their quantification using the CIE*Lab* system are shown in Figure **2**. Neat PLA changed from white to yellowish and became more opaque, typically attributed to increased crystallinity. In the case of the biocomposite, the brown color became less intense after weathering, due to the UV-induced degradation of the chromophore groups in the wood.

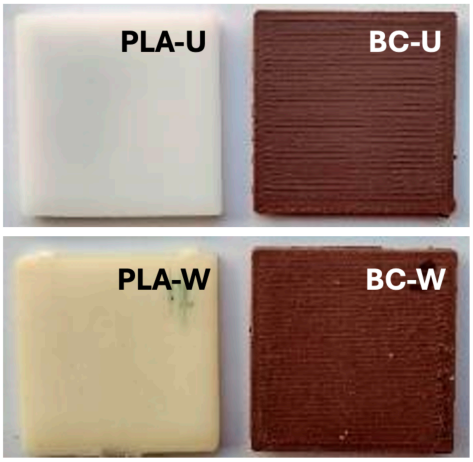

ΔL	-0.4	-0.8
ΔE	10.4	2.8

Figure 2: Color change of 3D-printed PLA and BC before (U) and after (W) accelerated weathering.

Before weathering, the samples exhibited higher lightness, with Δ*L* values decreasing by -0.4 for PLA and -0.8 for the biocomposite. The total color change (Δ*E*), indicating chromatic degradation, was greater in the neat PLA specimens due to the shift toward yellowish tones, compared to the biocomposite. As mentioned, the more pronounced color change in PLA can be attributed to increased crystallinity, induced by the elevated temperatures during accelerated weathering (González-López *et al*., 2020). Although a similar effect occurs in the biocomposite, as will be shown in the thermal properties section, the presence of wood reduces the visual impact of the color change of the PLA.

3.3. FTIR and Carbonyl Index

Figure **3** shows the infrared spectra of PLA and its biocomposite before and after weathering. In both cases, methyl group vibrations are observed, with stretching between 2970 and 2890 cm^{-1} and bending between 1430 and 1470 cm^{-1}. Ester groups exhibit signals at 1180, 1088, and 1040 cm^{-1}, along with carbonyl stretching vibrations around 1760 cm^{-1}.

After weathering, noticeable changes occur in the bands corresponding to the most relevant functional groups, which are the methyl and carbonyl groups. Chain scissions, attributed to Norrish type II reactions and hydrolysis, lead to an increase in carbonyl groups relative to methyl groups (Wang *et al*., 2013). These changes can be quantified using the carbonyl index (Equation 3), which is based on the area under the curve of the respective signals to provide a more meaningful and accurate comparison.

In both materials, PLA and the biocomposite, an increase in the carbonyl index (CI) was observed, indicating degradation on the surfaces exposed to weathering. Numerically, the CI increased from 3.2 to 7.2 for PLA and to 7.1 for the biocomposite. The slightly higher CI observed in pure PLA indicates a greater degree of degradation compared to the biocomposite, consistent with the porosity results.

3.2. Thermal Properties

Table **1** presents the thermal properties of the materials obtained by DSC, with the corresponding

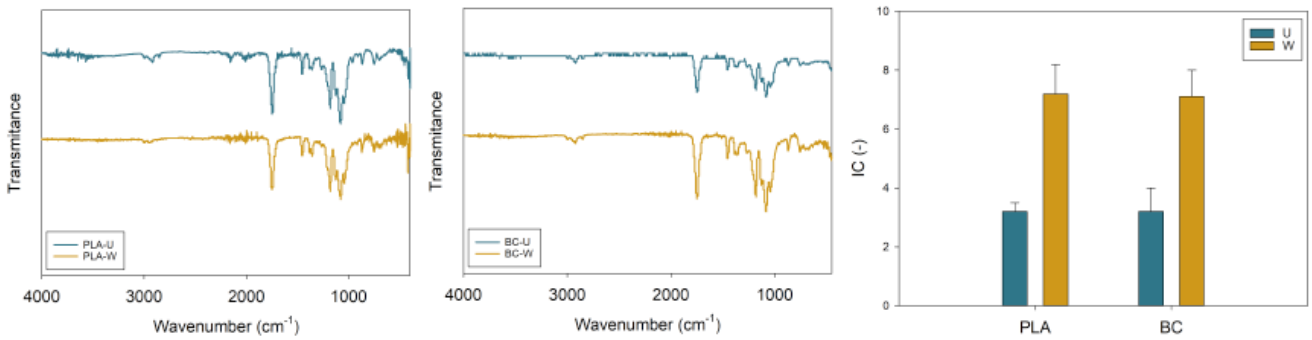

Figure 3: FTIR and carbonyl index of PLA and BC before (U) and after (W) accelerated weathering.

thermograms shown in Figure **4**. The glass transition temperature (T_g) remains practically the same for both materials and is unaffected by accelerated weathering. The melting temperature of PLA was 155 °C, and this temperature increased to 160 °C for the biocomposites. Weathering exposure reduces the melting temperature of both PLA and the biocomposite by 2–3 °C, due to polymer degradation that shortens the polymer chains and facilitates their movement. The cold crystallization temperature (T_c) of both materials, initially around 87 °C, is no longer observed after weathering, as recrystallization of the amorphous regions occurs in both PLA and the biocomposite during exposure. Sawpan *et al*., (2019) explained that exposure of PLA to UV light and elevated temperatures (above 50 °C) induces the rearrangement of amorphous regions into ordered structures, resulting in changes in the cold crystallization behavior. This leads to a significant increase in crystallinity in both materials: from 11.8% to 38.7% in PLA, and from 20.1% to 40.3% in the biocomposite. The biocomposite initially shows higher crystallinity due to the wood particles acting as nucleating agents during filament processing. The greater increase in crystallinity observed in neat PLA after weathering may be associated with the restricted chain mobility caused by the presence of fibers in the biocomposite (Sawpan *et al*., 2019). These crystallinity values are consistent with the color changes observed in both materials.

3.3. Mechanical Properties

The mechanical properties (tensile, flexural, and impact) of PLA and the biocomposite before and after

Table 1: Thermal Properties of 3D-Printed PLA and BC before (U) and after (W) Accelerated Weathering

Sample	T_g (ºC)		T_c (ºC)		T_m (ºC)		X_c (%)	
	U	W	U	W	U	W	U	W
PLA	58	58	87	-	155	152	11.8	38.7
BC	59	59	85	-	160	158	20.1	40.3

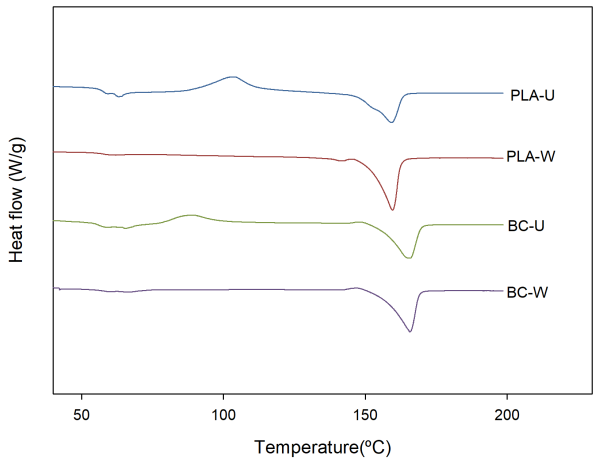

Figure 4: DSC thermograms of 3D-printed PLA and BC before (U) and after (W) accelerated weathering.

accelerated weathering are shown in Figure **5**. In general, the initial mechanical properties of the biocomposite are lower than those of neat PLA, mainly due to its higher porosity and likely poor interfacial adhesion between the wood particles and the PLA matrix. Similar results were reported by Cisneros-López *et al*. (2020), who found that the flexural properties were more than 50% higher when PLA was processed by injection molding compared to 3D printing.

However, after accelerated weathering, neat PLA exhibited a much greater reduction in mechanical properties due to its higher degradation, as also observed in the porosity values and the material morphology. In contrast, the biocomposite showed a slight increase in both tensile and flexural strength, rising from 25 to 28 MPa and from 36 to 41 MPa, respectively. This behavior is attributed to the minimal variation in porosity, which helps maintain the structural integrity of the biocomposite compared to neat PLA, as well as to the increased crystallinity. The positive effect of thermal annealing on tensile and flexural strength has been previously reported in systems such as PLA/coir and bamboo (Yaisun and Trongsatitkul, 2023). This effect, however, was not observed in the tensile modulus, where the porous structure of the material significantly influences its stiffness despite the increase in crystallinity.

Impact resistance was notably affected in both materials after weathering. Still, the reduction was much more pronounced in neat PLA due to the high discontinuity in its structure, dropping from 327 J m^{-1} to 111 J m^{-1}, representing a 65% loss. In contrast, the biocomposite experienced only a 27% reduction in this

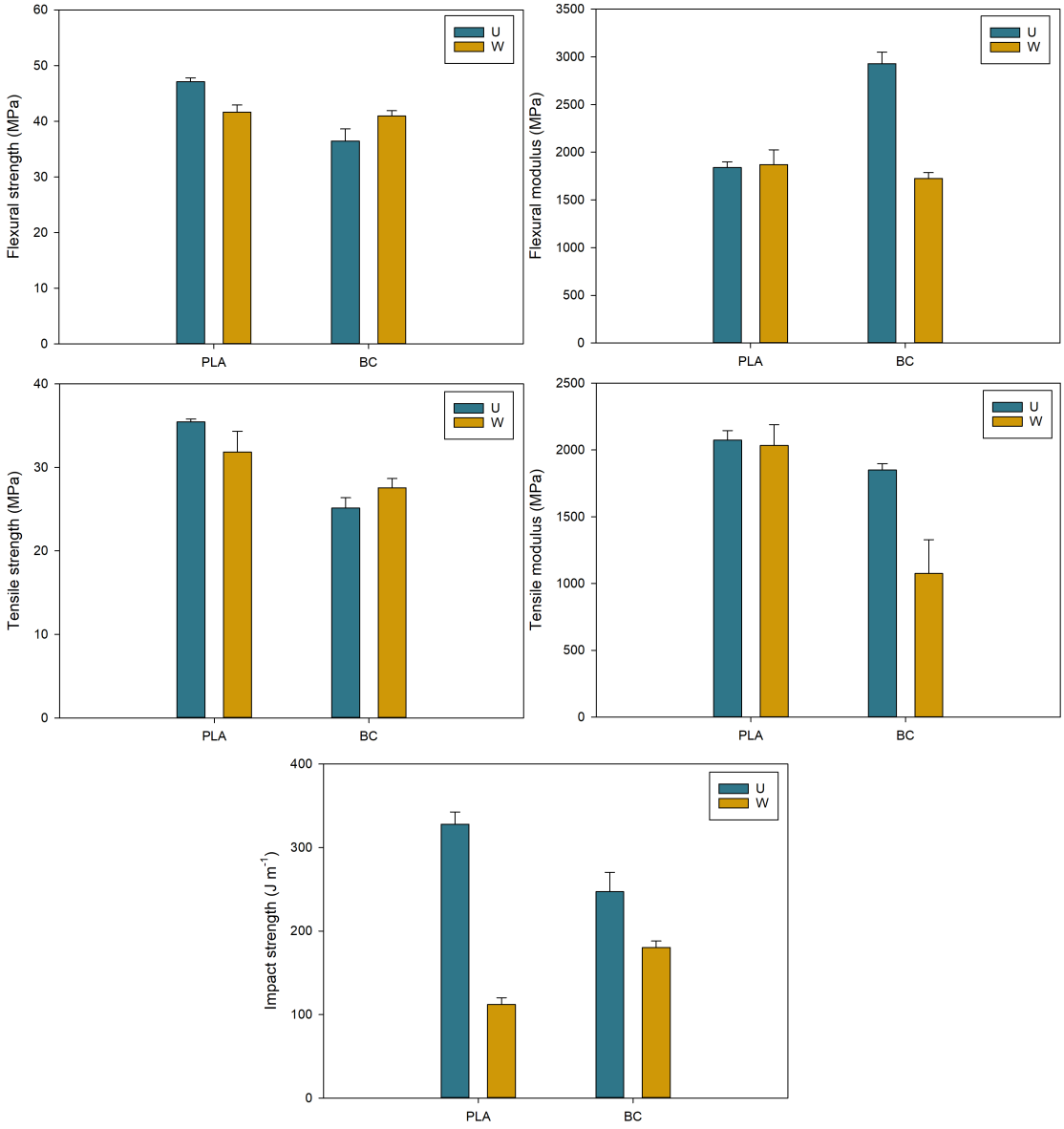

Figure 5: Mechanical properties of 3D-printed PLA and BC before (U) and after (W) accelerated weathering.

property. These results confirm that 3D-printed PLA undergoes greater degradation due to polymer chain scission and increased porosity resulting from the processing method and exposure to extreme accelerated weathering conditions.

3.4. Water Absorption

The results of water absorption and weight loss due to hydrolysis are presented in Figure **6**. As expected, the biocomposite exhibits higher water absorption than neat PLA, due to the hydrophilic nature of the wood particles, reaching values around 10%. It can also be observed that beyond a certain point, PLA experiences a significant weight loss, even resulting in negative values. This weight loss is attributed to the hydrolysis of the material, a degradation process that has been reported in other studies, which indicate that it can begin after relatively short immersion times (Medina *et al*., 2018; Drogu *et al*., 2021; Azka *et al*., 2024). Exposure to weathering did not alter the maximum water absorption of PLA up to 336 h. However, although weathering increases crystallinity, it also accelerates the onset of hydrolytic degradation due to the high porosity of the material.

In the case of the biocomposites, a reduction in both the maximum water absorption capacity and the absorption rate is also observed after weathering. This is due to the hydrolysis of the PLA matrix within the composite. Furthermore, a decrease in weight is observed after reaching a maximum at around 800 h, indicating that the rate of hydrolytic weight loss surpasses the rate of water absorption. Additionally, Figure **5** shows the total weight loss after 1000 h of immersion, followed by drying of the specimens. The protective effect of the wood particles against hydrolysis is evident, as the biocomposites show weight losses of less than 5%, while neat PLA shows values around 20%. This is attributed to the nucleating effect of the wood particles, which promote the formation of crystalline segments in the PLA, thereby inhibiting its hydrolysis. This effect was also reported by Jiang *et al*., (2020), who investigated the influence of short jute fibers on the hydrolysis of PLA.

3.5. Composting and Respirometry

The composting of biopolymers and biocomposites is a complex process that involves and depends on various fungi and bacteria. After the hydrolysis of high molecular weight chains, microorganisms produce extracellular enzymes (such as depolymerases, proteases, lipases, and cutinases), generating oligomers, dimers, and monomers that are further assimilated through the microbial membranes. Afterwards, the microorganisms use intracellular enzymes to mineralize these molecules (Zaaba and Jaafar, 2020).

Figure **7** shows the degree of disintegration by composting of the materials at different times, along with images of their structures. A progressive disintegration process is observed, which generally affects the neat PLA to a greater extent. After 10 days, the materials showed no significant changes; however, by day 24, a noticeable degree of disintegration was evident, reaching up to 31%. Dong *et al*. (2014) reported that the weight loss of PLA during composting becomes more significant after 18 days, when the microorganisms have adapted to the medium and composting conditions have improved.

By day 31, a more pronounced disintegration is observed, especially in the neat PLA samples. As previously mentioned, PLA is more susceptible to polymer chain scission via hydrolysis, particularly when the material has high porosity, as is the case with 3D printing. This effect is even more evident in weathered materials, where PLA specimens reach up to 80% disintegration after 85 days of composting. This is due to their previous exposure to UV, temperature, and humidity, which, as observed, increased their porosity. Also, neat PLA was probably more affected than the biocomposite due to the composting conditions and the specific microorganisms present, which more efficiently

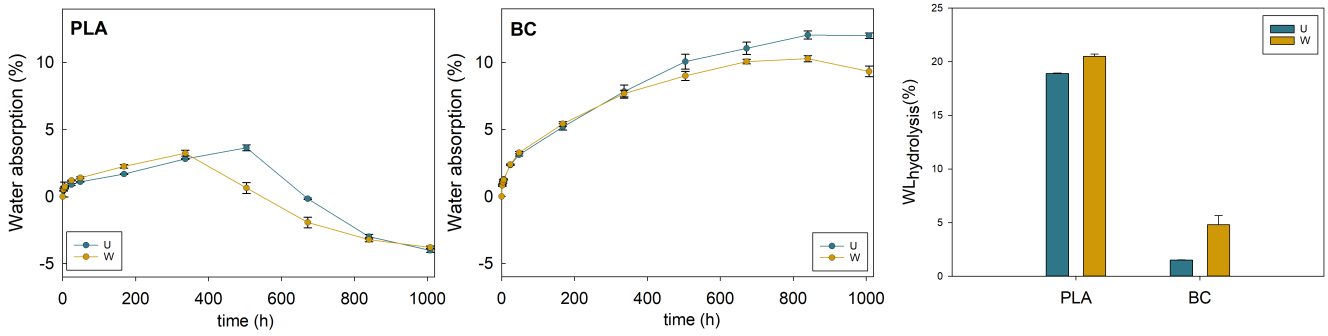

Figure 6: Water absorption and weight loss by hydrolysis of 3D-printed PLA and BC before (U) and after (W) accelerated weathering.

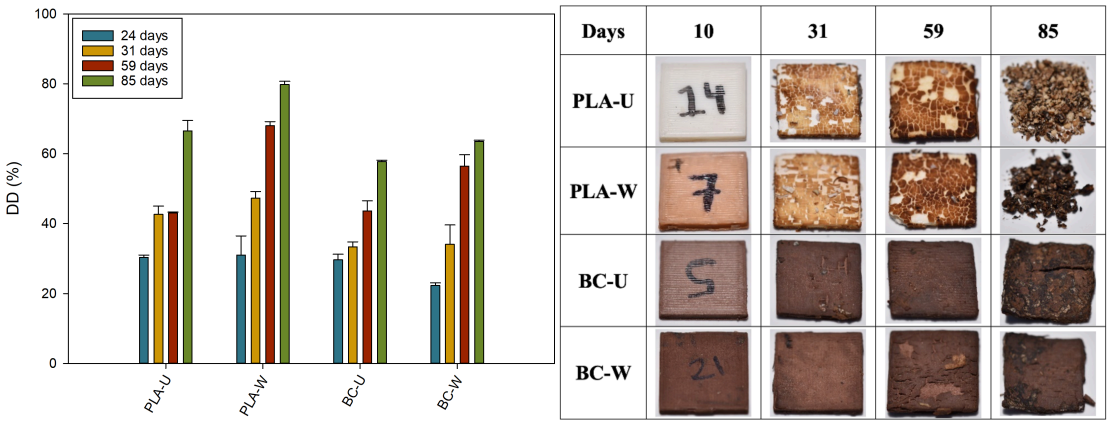

Figure 7: Disintegration under composting of 3D-printed PLA and BC before (U) and after (W) accelerated weathering.

degrade PLA than lignocellulosic materials, as well as the previously mentioned higher resistance of the biocomposite to hydrolysis, as observed in DSC and porosity results (Jiang *et al*., 2020; Dogru *et al*., 2021).

Both the disintegration values and the visual appearance of the specimens clearly indicated that the degradation of the materials was partial and led to the formation of small particles, some less than 1 mm in size, within the microplastic range (Van Cauwenberghe *et al*., 2015). Therefore, additional respirometry tests and microplastic analyses were necessary to characterize the biodegradation process of these materials better.

Figure **8** presents the microplastic fraction within the residual biopolymer recovered from the compost. As previously mentioned, the material was sieved to isolate particles ranging in size from 1000 µm to 1 µm. It is evident that neat PLA has a higher tendency to fracture, as indicated by a 26 % fraction of residual material with particle sizes falling within the microplastic range. Notably, this value remained essentially unchanged after weathering. This behavior is attributed to the high PLA susceptibility to hydrolysis and microbial attack. In contrast, it is noteworthy that the biocomposites generated significantly lower amounts of microplastics, less than 3%, even after being subjected to weathering.

Particle size analysis revealed that neat PLA fragments averaged 207 ± 49 µm in size, while those from its biocomposite averaged around 221 ± 71 µm. Exposure to weathering reduced the average particle size of residual PLA to 145 ± 50 µm. This indicates that porosity and prior weathering exposure promote greater hydrolytic degradation, shortening the PLA polymer chains and facilitating subsequent biotic degradation, resulting in smaller microplastic particles. On the other hand, the larger particle size of the biocomposite fragments, especially following weathering, further supports its resistance to hydrolysis. The presence of wood contributes to a more complex chemical composition and provides a protective effect, thereby reducing fragmentation. Along with the observed trends in weight loss and mineralization, these results suggest that biocomposites are effectively biodegradable materials. They demonstrate high mineralization rates and produce fewer microplastics in the short term compared to pure PLA. Even though they are still under extensive study, microplastics have been reported to cause several environmental effects, such as health problems due to ingestion and

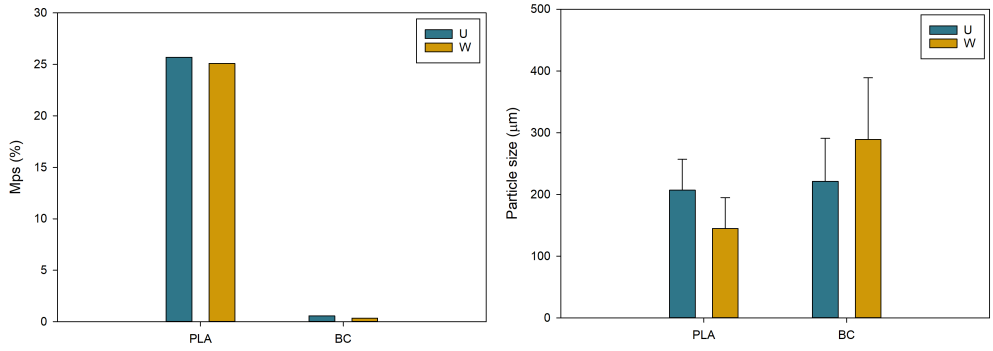

Figure 8: Microplastics generation and their particle size of 3D-printed PLA and BC before (U) and after (W) accelerated weathering.

accumulation, transport of toxic chemicals through adsorption, and soil quality degradation, among others (Van Cauwenberghe *et al*., 2015; Koelmans *et al*., 2016; Andrady *et al*., 2017). In addition, monitoring and reduced microplastic generation, even from biopolymers, is crucial to assess their large-scale application (Liao and Chen, 2021), to adapt composting facilities and conditions for safer end-of-life processes, and to enable and promote better circular economy integration of these materials.

Figure **9** presents the mineralization kinetics of 3D-printed neat PLA and its biocomposite. For neat PLA, a mineralization level of 35% was observed, while the biocomposite reached 36%. In the case of weathered PLA, mineralization increased to 39%, and for the weathered biocomposite, it reached 38%, slightly higher than their unexposed counterparts. This increase is again related to the higher porosity resulting from exposure to UV, temperature, and humidity. Interestingly, the maximum mineralization values for all materials fell within a narrow range (35%–39%), in contrast to the significantly larger differences observed in disintegration levels. This highlights that measuring weight loss alone during composting is not sufficient to fully characterize the biodegradation process of a material.

The mineralization values observed for 3D-printed PLA and its biocomposite were lower than those reported in the literature. For instance, Kalita *et al*. (2021) reported 80% mineralization for PLA reinforced with cellulose nanocrystals after 100 days. However, Husárová *et al*. (2014) conducted a study using PLA of varying molecular weights and found that PLA with higher molecular weight tends to show lower mineralization percentages compared to PLA with lower molecular weight. After 100 days, the difference in mineralization can be as much as 30%, depending also on the form in which the polymer is composted (*e.g*., powder, films, etc.). Also, it is important to consider that the PLA used in this study is the commercially known PLA+, whose additives to improve durability surely affect the rate of mineralization when compared with conventional PLA.

The mineralization kinetics were fitted using the Hill model, and the corresponding parameters are reported in Table **2**. The biocomposite exhibited a y_{max} value of 75%, higher than that of neat PLA, which reached 61%. As previously discussed, the wood particles increase porosity, making the material more prone to moisture absorption and microbial attack. However, for weathered PLA, a significant increase in y_{max} was observed, reaching 92%, while the biocomposite maintained a similar value to that of the unexposed material (74%). This behavior is once again attributed to the increased rate and susceptibility of PLA to hydrolysis after weathering, which is a critical step that precedes the biodegradation of the material (Husárová *et al*., 2014). Da Silva *et al*. (2024) compared different models to describe the biodegradation kinetics of

Table 2: Kinetic Parameters of the Hill Model for the Mineralization of 3D-Printed PLA and BC before (U) and after (W) Accelerated Weathering

Material	y_{max} (%)	k (days)	n (-)	R^2
PLA-U	61.5	71	1.1	0.993
BC-U	75.5	102	1.0	0.991
PLA-W	92.8	116	1.0	0.994
BC-W	74.7	85	1.1	0.992

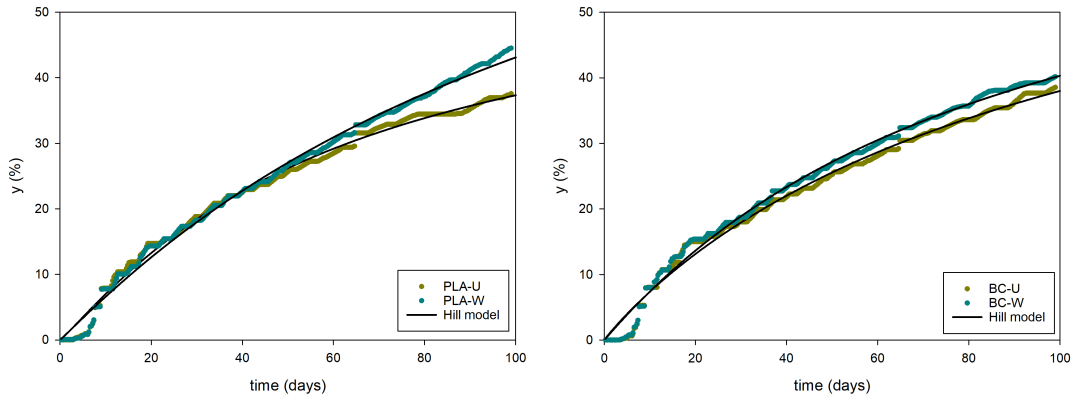

Figure 9: Mineralization kinetics under composting of 3D-printed PLA and BC before (U) and after (W) accelerated weathering.

polymers, such as first-order, subsequent first-order reactions, Michaelis-Menten-like, and Hill-like models. They reported that the Hill-like model was the most appropriate for describing the complex process of polymer biodegradation due to its ability to fit a wide range of biodegradation curves. The Hill model has also been successfully applied to describe the biodegradation of other biocomposites, such as PHB/agave and PHBV/agave systems (Gallardo-Cervantes *et al*., 2021).

4. CONCLUSIONS

The behavior of 3D-printed PLA and its PLA/wood biocomposite under abiotic and biotic degradation was evaluated. The porosity was initially higher in the biocomposite (12.5%) than in the neat PLA (7.5%). However, after weathering, the biocomposite was only slightly affected, while the porosity of the neat PLA increased to 13.2%. Additionally, color changes, weight loss from water immersion, and degradation of mechanical properties were generally more pronounced in the neat PLA than in the biocomposite. The wood particles act as nucleating agents and absorb water and UV radiation due to their chromophore groups, thereby reducing PLA hydrolysis and providing a protective effect in the biocomposite. The degree of disintegration and microplastic generation was lower in the biocomposite, without affecting mineralization.

ACKNOWLEDGEMENTS

One of the authors (Gómez-Comparán M.R.) acknowledges the Mexican National Council for Science and Technology for a scholarship.

DECLARATIONS

Conflict of Interest

The authors declare that they have no known competing financial interests or personal relationships that could have appeared to influence the work reported in this paper.

Ethical Approval

This article does not contain any studies with human participants or animals performed by any of the authors.

REFERENCES

[1] Andrady, A. L. (2017). The plastic in microplastics: A review. Marine Pollution Bulletin, 119(1), 12-22. https://doi.org/10.1016/j.marpolbul.2017.01.082

[2] Azka, M. A., Sapuan, S. M., Abral, H., Zainudin, E. S., & Aziz, F. A. (2024). An examination of recent research of water absorption behavior of natural fiber reinforced polylactic acid (PLA) composites: A review. International Journal of Biological Macromolecules, 268, 131845. https://doi.org/10.1016/j.ijbiomac.2024.131845

[3] Benhami, V. M. L., Longatti, S. M. de O., Moreira, F. M. de S., & Sena Neto, A. R. de. (2024). Biodegradation of poly(lactic acid) waste from 3D printing. Polímeros, 34(2), e20240013. https://doi.org/10.1590/0104-1428.20230058

[4] Bhagia, S., Bornani, K., Agarwal, R., Satlewal, A., Ďurkovič, J., Lagaňa, R., Bhagia, M., Yoo, C. G., Zhao, X., Kunc, V., Pu, Y., Ozcan, S., & Ragauskas, A. J. (2021). Critical review of FDM 3D printing of PLA biocomposites filled with biomass resources, characterization, biodegradability, upcycling and opportunities for biorefineries. Applied Materials Today, 24, 101078. https://doi.org/10.1016/j.apmt.2021.101078

[5] Chopra, S., Pande, K., Puranam, P., Deshmukh, A. D., Bhone, A., Kale, R., Galande, A., Mehtre, B., Tagad, J., & Tidake, S. (2023). Explication of mechanism governing atmospheric degradation of 3D-printed poly(lactic acid) (PLA) with different in-fill pattern and varying in-fill density. RSC Advances, 13(11), 7135-7152. https://doi.org/10.1039/D2RA07061H

[6] Cisneros-López, E. O., Pal, A. K., Rodriguez, A. U., Wu, F., Misra, M., Mielewski, D. F., Kiziltas, A., & Mohanty, A. K. (2020). Recycled poly(lactic acid)-based 3D printed sustainable biocomposites: A comparative study with injection molding. Materials Today Sustainability, 7-8, 100027. https://doi.org/10.1016/j.mtsust.2019.100027

[7] da Silva, S. A., Faccin, D. J. L., & Cardozo, N. S. M. (2024). A kinetic-based criterion for polymer biodegradability applicable to both accelerated and standard long-term composting biodegradation tests. ACS Sustainable Chemistry & Engineering, 12(32), 11856-11865. https://doi.org/10.1021/acssuschemeng.3c03837

[8] Dogru, A., Sozen, A., Neser, G., & Seydibeyoglu, M. O. (2021). Effects of aging and infill pattern on mechanical properties of hemp reinforced PLA composite produced by fused filament fabrication (FFF). Applied Science and Engineering Progress, 14(4), 651-660. https://doi.org/10.14416/j.asep.2021.08.007

[9] Dong, Y., Ghataura, A., Takagi, H., Haroosh, H. J., Nakagaito, A. N., & Lau, K. T. (2014). Polylactic acid (PLA) biocomposites reinforced with coir fibres: Evaluation of mechanical performance and multifunctional properties. Composites Part A: Applied Science and Manufacturing, 63, 76-84. https://doi.org/10.1016/j.compositesa.2014.04.003

[10] Figueroa-Velarde, V., Diaz-Vidal, T., Cisneros-López, E. O., Robledo-Ortiz, J. R., López-Naranjo, E. J., Ortega-Gudiño, P., & Rosales-Rivera, L. C. (2021). Mechanical and physicochemical properties of 3D-printed agave fibers/poly(lactic acid) biocomposites. Materials, 14(11), 3111. https://doi.org/10.3390/ma14113111

[11] Gallardo-Cervantes, M., González-García, Y., Pérez-Fonseca, A. A., González-López, M. E., Manríquez-González, R., Rodrigue, D., & Robledo-Ortíz, J. R. (2021). Biodegradability and improved mechanical performance of polyhydroxyalkanoates/agave fiber biocomposites compatibilized by different strategies. Journal of Applied Polymer Science, 138(12), 50182. https://doi.org/10.1002/app.50182

[12] González-López, M. E., Martín Del Campo, A. S., Robledo-Ortíz, J. R., Arellano, M., & Pérez-Fonseca, A. A. (2020). Accelerated weathering of poly (lactic acid) and its biocomposites: A review. Polymer Degradation and Stability, 179, 109290. https://doi.org/10.1016/j.polymdegradstab.2020.109290

[13] Gramazio, F., Kohler, M., & Willmann, J. (2014). The robotic touch: How robots change architecture. Park Books.

[14] Husárová, L., Pekař, Š., Stloukal, P., Kucharzcyk, P., Verney, V., Commereuc, S., Ramone, A., & Koutny, M. (2014). Identification of important abiotic and biotic factors in the biodegradation of poly (L-lactic acid). International Journal of

Biological Macromolecules, 71, 155-162. https://doi.org/10.1016/j.ijbiomac.2014.04.050

[15] Jain, P. K., & Jain, P. K. (2021). Use of 3D printing for home applications: A new generation concept. Materials Today: Proceedings, 43(1), 605-607. https://doi.org/10.1016/j.matpr.2020.12.145

[16] Jiang, N., Li, Y., Li, Y., Yu, T., Li, Y., Li, D., Xu, J., Wang, C., & Shi, Y. (2020). Effect of short jute fibers on the hydrolytic degradation behavior of poly(lactic acid). Polymer Degradation and Stability, 178, 109214. https://doi.org/10.1016/j.polymdegradstab.2020.109214

[17] Joseph, T. M., Kallingal, A., Suresh, A. M., Sreekumar, P. R. S., Paul, M. T. P., & John, H. (2023). 3D printing of polylactic acid: Recent advances and opportunities. The International Journal of Advanced Manufacturing Technology, 125, 1015-1035. https://doi.org/10.1007/s00170-022-10795-y

[18] Kalita, N. K., Sarmah, A., Bhasney, S. M., Kalamdhad, A., & Katiyar, V. (2021). Demonstrating an ideal compostable plastic using biodegradability kinetics of poly(lactic acid) (PLA) based green biocomposite films under aerobic composting conditions. Environmental Challenges, 3, 100030. https://doi.org/10.1016/j.envc.2021.100030

[19] Koelmans, A.A., Bakir, A., Burton, G.A., & Janssen, C.R. (2016). Microplastic as a vector for chemicals in the aquatic environment: Critical review and model-supported reinterpretation of empirical studies. Environmental Science & Technology, 50(7), 3315-3326. https://doi.org/10.1021/acs.est.5b06069

[20] La Fuente Arias, C. I., González-Martínez, C., & Chiralt, A. (2024). Biodegradation behavior of poly(3-hydroxybutyrate-co-3-hydroxyvalerate) containing phenolic compounds in seawater in laboratory testing conditions. Science of The Total Environment, 944, 173920. https://doi.org/10.1016/j.scitotenv.2024.173920

[21] Liao, J., & Chen, Q. (2021). Biodegradable plastics in the air and soil environment: Low degradation rate and high microplastics formation. Journal of Hazardous Materials, 418, 126329. https://doi.org/10.1016/j.jhazmat.2021.126329

[22] Lin, W., Xie, G., & Qiu, Z. (2019). Effects of ultraviolet aging on properties of wood flour-poly(lactic acid) 3D printing filaments. BioResources, 14(4), 8689-8700. https://doi.org/10.15376/biores.14.4.8689-8700

[23] Lucas, N., Bienaime, C., Belloy, C., Queneudec, M., Silvestre, F., & Nava-Saucedo, J. E. (2008). Polymer biodegradation: Mechanisms and estimation techniques: A review. Chemosphere, 73(4), 429-442. https://doi.org/10.1016/j.chemosphere.2008.06.064

[24] Martín Del Campo, A. S., Robledo-Ortíz, J. R., Arellano, M., Rabelero, M., & Pérez-Fonseca, A. A. (2021). Accelerated weathering of polylactic acid/agave fiber biocomposites and the effect of fiber-matrix adhesion. Journal of Polymers and the Environment, 29(3), 937-947. https://doi.org/10.1007/s10924-020-01936-z

[25] Medina, J., Roche, Y., Maldonado, O., Hernández, J. C., & Zapata, C. (2018). Hydrolytic degradation and biodegradation of binary mixes of polylactic acid (PLA) with plastic residues. Revista Ingeniería UC, 25(2), 248-258.

[26] Meereboer, K. W., Misra, M., & Mohanty, A. K. (2020). Review of recent advances in the biodegradability of polyhydroxyalkanoate (PHA) bioplastics and their composites. Green Chemistry, 22(17), 5519-5558. https://doi.org/10.1039/D0GC01647K

[27] Ning, X., Liu, T., Wu, C., & Wang, C. (2021). 3D printing in construction: Current status, implementation hindrances, and development agenda. Advances in Civil Engineering, 2021, Article 6665333. https://doi.org/10.1155/2021/6665333

[28] Petchwattana, N., Channuan, W., Naknaen, P., & Narupai, B. (2019). 3D printing filaments prepared from modified poly(lactic acid)/teak wood flour composites: An investigation on the particle size effects and silane coupling agent compatibilization. Journal of Physical Science, 30(2), 169-188. https://doi.org/10.21315/jps2019.30.2.10

[29] Sawpan, M., Islam, M. R., Beg, M. D. H., & Pickering, K. (2019). Effect of accelerated weathering on physico-mechanical properties of polylactide bio-composites. Journal of Polymers and the Environment, 27(5), 942-955. https://doi.org/10.1007/s10924-019-01405-2

[30] Van Cauwenberghe, L., Devriese, L., Galgani, F., Robbens, J., & Janssen, C.R. (2015)

[31] Microplastics in sediments: A review of techniques, occurrence and effects. Marine Environmental Research, 111, 5-17. https://doi.org/10.1016/j.marenvres.2015.06.007

[32] Wang, D. K., Varanasi, S., Fredericks, P. M., Hill, D. J. T., Symons, A. L., Whittaker, A. K., & Rasoul, F. (2013). FT-IR characterization and hydrolysis of PLA-PEG-PLA based copolyester hydrogels with short PLA segments and a cytocompatibility study. Journal of Polymer Science, Part A: Polymer Chemistry, 51(24), 5163-5176. https://doi.org/10.1002/pola.26930

[33] Yaisun, S., & Trongsatitkul T. (2023). PLA-based hybrid biocomposites: Effects of fiber type, fiber content, and annealing on thermal and mechanical properties. Polymers, 15, 4106. https://doi.org/10.3390/polym15204106

[34] Yang, S., & Du, P. (2022). The application of 3D printing technology in furniture design. Scientific Programming, 2022, 1960038. https://doi.org/10.1155/2022/1960038

[35] Yin, H., Qu, M., Zhang, H., & Lim, Y. (2018). 3D printing and buildings: A technology review and future outlook. Technology, Architecture + Design, 2(1), 94-111. https://doi.org/10.1080/24751448.2018.1420968

[36] Zaaba, N.F., & Jaafar, M. (2020). A review on degradation mechanisms of polylactic acid: Hydrolytic, photodegradative, microbial, and enzymatic degradation. Polymer Engineering and Science, 60, 2061-2075. https://doi.org/10.1002/pen.25511

https://doi.org/10.66000/2819-828X.2025.01.02

© 2025 Pérez-Fonseca *et al.*
This is an open-access article licensed under the terms of the Creative Commons Attribution License (http://creativecommons.org/licenses/by/4.0/), which permits unrestricted use, distribution, and reproduction in any medium, provided the work is properly cited.